Adaptive Input Shaper for Payload Swing Control of a 5-DOF Tower Crane with Parameter Uncertainties and Obstacle Avoidance

S. M. Fasih ur Rehman[1,2], Z. Mohamed[1*], A. R. Husain[1], L. Ramli[3], M. A. Abbasi[2], W. Anjum[2], M. H. Shaheed[4]

[1]Faculty of Electrical Engineering, Universiti Teknologi Malaysia, Johor, Malaysia
[2]Department of Electronic Engineering, Faculty of Engineering, The Islamia University of Bahawalpur, Punjab, Pakistan
[3]Faculty of Engineering and Built Environment, Universiti Sains Islam Malaysia, Negeri Sembilan, Malaysia
[4]School of Engineering and Materials Science, Queen Mary University of London, London, UK

*Corresponding author: zahar@fke.utm.my

ABSTRACT

This paper proposes an adaptive input shaper for swing control of a five degrees of freedom tower crane under various parameter uncertainties together with payload hoisting and simultaneous motions. The real-time adaptive mechanism is designed using neural network and the shaper parameters can be updated based on current crane's parameters. This approach avoids the requirement for re-design of controllers as in the conventional technique. Experiments are conducted to assess effectiveness of the controller under challenging scenarios up to 100% changes in the system's natural frequency. These involve different speeds and payload masses, payload hoisting, and distances of trolley and jib. Results demonstrate that the shaper is robust against parameter uncertainties and its superiority is confirmed with an improvement of at least 50% as compared to a comparative robust shaper. The shaper also provides a satisfactory performance under obstacle avoidance where payload lifting and lowering are performed within a single manoeuvre.

Keywords: Feedforward control; Input shaping; Neural network; Swing control; Tower crane.

1. INTRODUCTION

Cranes are one of the most widely used machines in industries for transportation of heavy and hazardous loads to a desired destination. In a construction industry, a tower crane has proved its usefulness for transporting heavy building materials and the small footprint with a wide working area makes it suitable for constructing skyscrapers. Moreover, its characteristics of long jib, high lifting height and heavy lifting ability are advantages in constructions of high-

rise building, bridges and other structures. Many difficult construction tasks can be automated using the tower cranes which result in a faster completion time. A five degrees of freedom (5-DOF) tower crane involves translational motion of trolley, rotational motion of jib, payload hoisting up and down, and payload pendulation angles in x and y-axes. It is an underactuated system as the number of actuators is less than the degree of freedom. Generally, a fast motion of a tower crane with minimum payload swing is highly desirable to increase productivity, and to ensure safety. However, efficient control of the payload sway is very challenging as the sway is affected by many factors. The dynamic behaviour of the crane is complicated due to a nonlinear coupling of the slew and translational motions, and the payload also pendulates in a circular pattern. Moreover, the payload swing dynamics change during essential payload hoisting operations as the length of cable attached to the payload varies. The magnitude of the payload swing is also affected by the payload mass, motion speed and distances of the trolley and jib movements. For example, a fourfold increase in the trolley or jib displacement doubles the operational time as the operator needs to wait longer time for the payload oscillation to settle down [1]. In addition, the control challenge increases under simultaneous trolley and jib motions together with payload hoisting.

Many researchers have proposed different techniques to minimise or eliminate the payload swing with varying levels of success. The most notable techniques based on feedback control are robust control [2, 3], nonlinear control [4, 5], model predictive control [6, 7], sliding mode control [8, 9, 10], artificial intelligent control [11, 12, 13, 14], and adaptive control [15, 16]. Recently, a neuroadaptive controller for a tower crane with simultaneous output and velocity constraints was proposed [17]. The closed-loop control schemes provide a good and robust performance, but they required installation of additional sensors, good mathematical model of the system and were difficult to implement. Besides, open loop control approaches that include input shaping [18, 19, 20], command smoothing [21, 22] and command filtering [23] techniques have also been reported. The control approach is easy to implement and does not need additional sensors. However, it requires an accurate dynamic model, and it is not robust to system uncertainties and disturbances. In addition, as the input shaping techniques were designed based on a linear system, their performance degraded when used for nonlinear and time-varying systems. It was found in the literature that most of the work reported on open loop control involves implementations on gantry and overhead cranes and not much on a rotary/tower crane. This may be due to the nonlinear nature and rotational motion of jib/boom which increase the difficulty for sway control.

For efficient sway control, a shaper that is robust to parameters that affect the sway magnitudes and dynamics is required. Input shapers that were robust to changes in the crane parameters have previously been designed in [20, 24, 25, 26]. In [27], a shaper designed based on the Average Operating Frequency (AOF) of initial and final cable lengths was shown to be more efficient in suppressing the payload oscillation. An adaptive Unity Magnitude Zero Vibration (UMZV) shaper which can handle changes in the crane dynamics was also proposed in [24]. It was found that there is a deficiency of robust shaper in the literature especially for a tower crane, and most of the proposed robust shaping techniques deal with the gantry and overhead cranes. In a recent work [20], a neural network-based adaptive input shaper was proposed for payload swing suppression of a tower crane. However, the work only considered the changes in the cable length and payload mass to update the shaper parameters. It is desirable to design a shaper which is robust to many factors including the trolley displacement and jib rotation angle. It is also a great advantage to ensure a low payload sway regardless of trolley displacement and jib rotation distances, and during an obstacle avoidance operation.

In this work, an adaptive Zero Vibration Derivative (ZVD) shaper that can adapt to parameter uncertainties for efficient sway control of a 5-DOF tower crane is proposed. The shaper is based on Neural Network (NN) which has the capability to learn and predict optimal shaper parameters based on cable length, payload mass, trolley displacement and jib angle. Experiments are conducted on a laboratory crane under various scenarios to evaluate the controller performance in terms of the overall and residual payload sways. An obstacle avoidance operation is also examined to further investigate its robustness. For comparisons, robust Extra Insensitive (EI) shapers based on AOF are designed and implemented for each manoeuvre. The main contributions of this work as compared to the existing literature are:

a) A new adaptive input shaping design for payload swing control by considering varying cable length, payload mass and distances of trolley displacement and jib rotation. In the best of author's knowledge, there is no work that consider all the important factors together, especially for a 5-DOF tower crane.
b) The adaptive shaper can handle simultaneous crane motions of trolley displacement, jib rotation and payload lifting and lowering. This type of study that involves the challenging cases is limited in the literature.
c) The proposed shaper is able to provide acceptable performance under an obstacle avoidance operation that involves payload lifting and lowering in a single manoeuvre together with trolley displacement and jib rotation motions. Not much work has been done on evaluating this scenario in the literature.

2. TOWER CRANE MODEL

Figure 1 shows the schematic diagram of a 5-DOF tower crane considered in this work. The cylindrical coordinate system is used to define the trolley displacement $r(t)$, jib rotational angle $\gamma(t)$ and position of payload $P(t)$ attached to an inextensible cable with varying length of $L(t)$. $\theta(t)$ and $\phi(t)$ are the payload swing angles. The position of the payload $P(t)$ in a three-dimensional (3D) space can be represented in terms of unit vectors $\hat{x}$, $\hat{y}$ and $\hat{z}$ along the x, y and z-axes, as

$$P(t) = [r(t) - L(t)\cos\theta(t)\sin\phi(t)]\hat{x} + [L(t)\sin\theta(t)]\hat{y} - [L(t)\cos\theta(t)\cos\phi(t)]\hat{z} \quad (1)$$

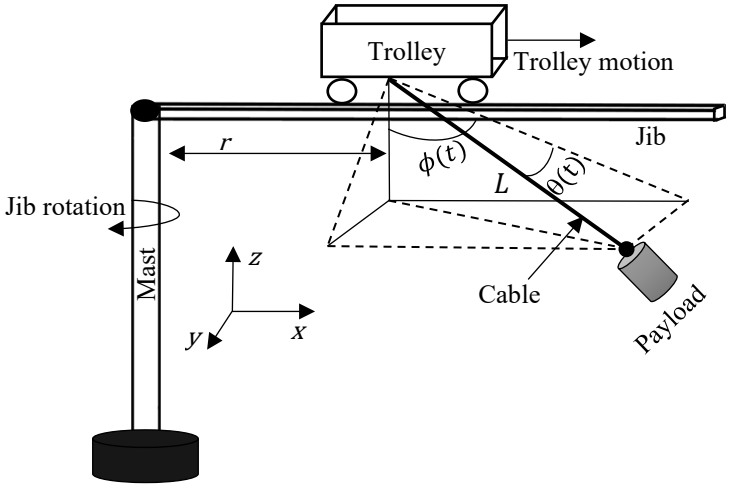

Figure 1: Tower crane schematic diagram

Therefore, the payload velocity can be obtained as

$$\begin{aligned}\dot{P}(t) = \big[\dot{r}(t) - \dot{L}(t)\sin\phi(t)\cos\theta(t) - L(t)\big(\dot{\gamma}(t)\sin\theta(t) - \dot{\theta}(t)\sin\theta(t)\sin\phi(t) \\ + \dot{\phi}(t)\cos\theta(t)\cos\phi(t)\big)\big]\hat{x} + \big[\dot{L}(t)\sin\theta(t) + r(t)\dot{\gamma}(t) + L(t)\cos\theta(t) \\ \big(\dot{\theta}(t) - \dot{\gamma}(t)\sin\phi(t)\big]\hat{y} + \big[-\dot{L}(t)\cos\theta(t)\cos\phi(t) + L(t) \\ \big(\dot{\theta}(t)\sin\theta(t)\cos\phi(t) + \dot{\phi}(t)\sin\phi(t)\cos\theta(t)\big)\big]\hat{z}\end{aligned} \quad (2)$$

The kinetic energy of the payload having a mass m can be calculated as

$$K_E = \frac{1}{2}m\big[\dot{P}(t).\dot{P}(t)\big] \quad (3)$$

and the potential energy of payload can be obtained as

$$P_E = -mgL(t)\cos\theta\,(t)\cos\phi\,(t) \quad (4)$$

where g is the gravitational constant. By using the Lagrange equation, payload accelerations along both payload swing angles can be obtained as

$$\ddot{\theta} = -\frac{1}{L}\left(\frac{\beta_1\dot{\theta}}{Lm} + 2\dot{L}\dot{\theta} - 2L\dot{\phi}\dot{\gamma}\cos^2\theta\cos\phi + \frac{1}{2}L\dot{\phi}^2\sin 2\theta - 2\dot{L}\dot{\gamma}\sin\phi + r\ddot{\gamma}\cos\theta - r\dot{\gamma}^2\sin\theta\sin\phi - L\ddot{\gamma}\sin\phi + g\sin\theta\cos\phi + 2\dot{r}\dot{\gamma}\cos\theta + \ddot{r}\sin\theta\sin\phi - \frac{1}{2}L\dot{\gamma}^2\sin 2\theta\cos^2\phi\right) \tag{5}$$

$$\ddot{\phi} = \frac{-1}{L\cos^2\theta}\left(\frac{\beta_2\dot{\phi}}{Lm} - L\dot{\theta}\dot{\phi}\sin 2\theta + 2L\dot{\theta}\dot{\gamma}\cos^2\theta\cos\phi + \dot{L}\dot{\gamma}\sin 2\theta\cos\phi - r\dot{\gamma}^2\cos\theta\cos\phi - \frac{1}{2}L\dot{\gamma}^2\cos^2\theta\sin 2\phi - \ddot{r}\cos\theta\cos\phi + 2\dot{L}\dot{\phi}\cos^2\theta + g\cos\theta\sin\phi + \frac{1}{2}L\ddot{\gamma}\sin 2\theta\cos\phi\right) \tag{6}$$

where β_1 and β_2 are the compensating factors and are taken as 0.01 and 0.0015. The tower crane is excited by the inputs $\ddot{r}$, $\ddot{\gamma}$ and $\dot{L}$ for trolley, jib and hoisting movements, respectively. Equations (5) and (6) show that the payload swings along both angles are nonlinear and coupled. In this work, the crane's dynamic equations are simulated to obtain payload swing responses in *x* and *y*-axes under various crane parameters and operations. The collected data based on the system responses will then be used for training of NN and for development of an adaptive shaper.

3. INPUT SHAPING DESIGN

The input shaping technique is an open loop control used to prevent the resonant output of the system by modulating the control signal. Input shaper consists of a train of impulses with a specific magnitude and time delay. The shaper's parameters are calculated so that the resultant sum of motion-induced oscillations is zero. Practically, input shaping is implemented in an open loop configuration by exciting the system with the shaped input obtained after convolving the baseline command with the shaper impulses.

The simplest form of shaper with only two impulses is called Zero Vibration (ZV) shaper. The robustness of the shaper can be increased by taking the derivative of residual vibration equal to zero with respect to the frequency of residual vibration, and the resultant shaper is

known as ZVD. The ZVD shaper consists of three impulses, in which the pulse amplitude A_i and time delay t_i can be calculated as

$$\begin{bmatrix} A_i \\ t_i \end{bmatrix} = \begin{bmatrix} \frac{1}{1+2K+K^2} & \frac{2K}{1+2K+K^2} & \frac{K^2}{1+2K+K^2} \\ 0 & \frac{\pi}{\omega_d} & \frac{2\pi}{\omega_d} \end{bmatrix} \tag{7}$$

where

$$\omega_d = \omega_n\sqrt{1-\zeta^2} \tag{8}$$

$$K = e^{\left(\frac{-\zeta\pi}{\sqrt{1-\zeta^2}}\right)} \tag{9}$$

ζ and ω_n are the damping ratio and the natural frequency of the system respectively. A vibration free system response can be obtained if suitable magnitudes and time delays are selected.

4. ROBUST INPUT SHAPERS

The effectiveness of input shapers in suppressing the oscillations induced by the motion is highly dependent on the accuracy of the obtained system's natural frequency and damping ratio. In addition, as an input shaper is derived based on a linear second order system, its effectiveness is negatively affected when applied to a higher order nonlinear system such as the tower crane. Moreover, parameters of the tower crane vary during operations. Previous work has shown that the ZVD shaper cannot limit the residual system vibration by 5% when parameters change more than $\pm$14% [28].

In this work the following factors are considered:

a) Payload hoisting (lifting and lowering) with varying cable length.
b) Different payload masses.
c) Several distances of trolley displacement and jib rotation.
d) Obstacle avoidance by combining payload lifting and lowering operations.
e) Simultaneous motions of the trolley, jib and payload lifting/lowering.

As a robust shaper is essential to ensure an effective sway reduction, a mechanism to automatically update the shaper parameters with changing system dynamics is required. Multiple adaptive approaches have been considered for implementation with the open loop

control. Among suitable approaches were fuzzy logic and NN as both can deal with real time data. However, the fuzzy logic design requires finding suitable membership functions, fine tuning of parameters and usually work best when the solution can be defined in a linguistic form, whereas the NN can provide a good performance when the input and output relation is nonlinear and with changing system parameters. Therefore, a robust shaper based on NN is proposed in this work for payload swing control of a 5-DOF tower crane under the effects listed in (a) - (e). In the literature, NN has been utilised to solve several engineering related problems [19]. A robust EI shaper designed using AOF is also designed for performance comparison.

4.1 Neural Network (NN) Based Shaper Design

In this work, the proposed adaptive shapers considered a similar ZVD shaper with three impulses, but their parameters can be updated in real time with respect to the changing system parameters. Therefore, the proposed method has an advantage over the conventional ZVD shaper that it provides an enhanced robustness with the same number of impulses and without increasing the shaper duration.

The design of the proposed NN-ZVD shaper with optimal parameters consists of the following steps:

a) Simulations of the tower crane were carried out using the dynamic model in Equations (5) and (6). The parameters used were g = 9.81 m/s^2, payload masses of 50 g, 150 g, 250 g and 350 g, and cable lengths of 0.1 m to 0.9 m. The trolley and jib were moved to different positions from 0.1 m to 0.5 m and 10 to 50 degrees, respectively.

b) System responses in x and y-axes were observed, and the natural frequencies and damping ratios were calculated.

c) Step (a) was repeated to collect results of the natural frequencies and damping ratios for all possible combinations of jib angle and trolley displacements with a difference of 10 degrees and 0.1 m, respectively. The same data is collected for all four payloads with a cable length variation of 0.1 m.

d) The data collected in steps (a), (b) and (c) against the four different variables of payload mass, cable length, jib angle and trolley displacement were used to calculate optimal ZVD parameters using Equation (7). To suppress the payload swing along two axes, two ZVD shapers are required, each having three impulses with magnitudes (A_1_x, A_2_x, $A_3\_x, A_1\_y, A_2\_y, A_3\_y$) and time delays ($\Delta T\_x$, ΔT_y). Table 1 shows some of the collected data together with the calculated ZVD shaper parameters.

e) The data shown in Table 1 was then used for the development of NN. The training process mapped the NN with nonlinear relationship between the input and output values of the parameters.

f) Figure 2 shows a diagram for implementation of the NN-ZVD. The NN calculates the optimal shaper parameters based on the training process by using data generated in step (d). Thus, the shaper was able to adapt and achieve robustness against all the factors and minimising the payload swing of both axes under tangential and radial inputs.

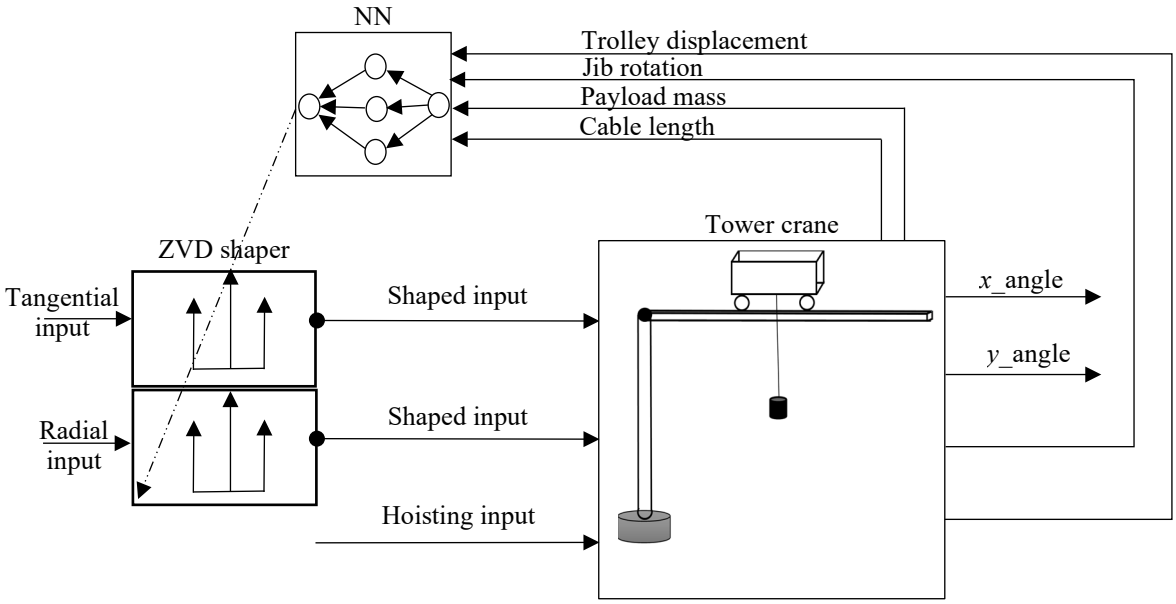

Figure 2: NN-ZVD implementation of tower crane.

Table 1: Data collection for NN

Payload mass (g)	Jib rotation (deg)	Trolley (m)	Length (m)	axis	A_1	A_2	A_3	ΔT (s)
50	10	0.1	0.1	x	0.303	0.5	0.197	0.450
				y	0.280	0.5	0.221	0.450
50	20	0.2	0.2	x	0.302	0.5	0.198	0.500
				y	0.278	0.5	0.222	0.500
150	30	0.3	0.3	x	0.260	0.5	0.240	0.550
				y	0.255	0.5	0.244	0.550
150	40	0.4	0.4	x	0.257	0.5	0.243	0.635
				y	0.253	0.5	0.247	0.635
250	50	0.5	0.5	x	0.253	0.5	0.247	0.710
				y	0.251	0.5	0.249	0.705

250	10	0.1	0.6	x	0.252	0.5	0.249	0.780
				y	0.251	0.5	0.249	0.775
350	20	0.2	0.7	x	0.251	0.5	0.249	0.840
				y	0.250	0.5	0.250	0.845
350	30	0.3	0.8	x	0.251	0.5	0.249	0.900
				y	0.250	0.5	0.249	0.915

The collected data as in Table 1 is utilised to train NN which maps the nonlinearity between the inputs and outputs. Therefore, based on a new set of inputs, ZVD shaper can be updated in real time with optimal parameters. The training process of the NN was performed by using the Bayesian regularisation as it has the ability to achieve good generalisation of the complex data of a nonlinear system. This algorithm also works best when the target is within the range of [-1,1]. From the total collected data, 80% and 20% were used for training and testing respectively. The Bayesian regularisation used the Levenberg-Marquardt technique to optimize the weight and bias values based on minimizing the linear combination of link weights and squared errors. By using this technique and by limiting the maximum number of iterations, overfitting can be avoided. Moreover, to ensure that NN is able to establish dominant trends among various input and output parameters which avoid the issue of underfitting, adequate numbers of observations were used during the training.

The NN design has four input neurons for cable length, payload mass, trolley displacement and jib angle, as shown in Figure 3. As described in step (d), six impulse magnitudes and two time delays are required for the design of two ZVD shapers. It can be noted in Table 1 that the impulse values of A_2 for both axes are 0.5 for all possible combinations of inputs, and since the delays of the last two impulses are multiple of the first impulse delay, only six outputs were generated from NN to reduce the computational burden. The six NN outputs were magnitudes of impulses (A_1_x, A_3_x, A_1_y, A_3_y) and time delays (ΔT_x, ΔT_y). Based on the higher number of features in the collected data, the complexity of the crane system model and the actuation input limitation, 20 hidden neurons were used to achieve satisfactory performance.

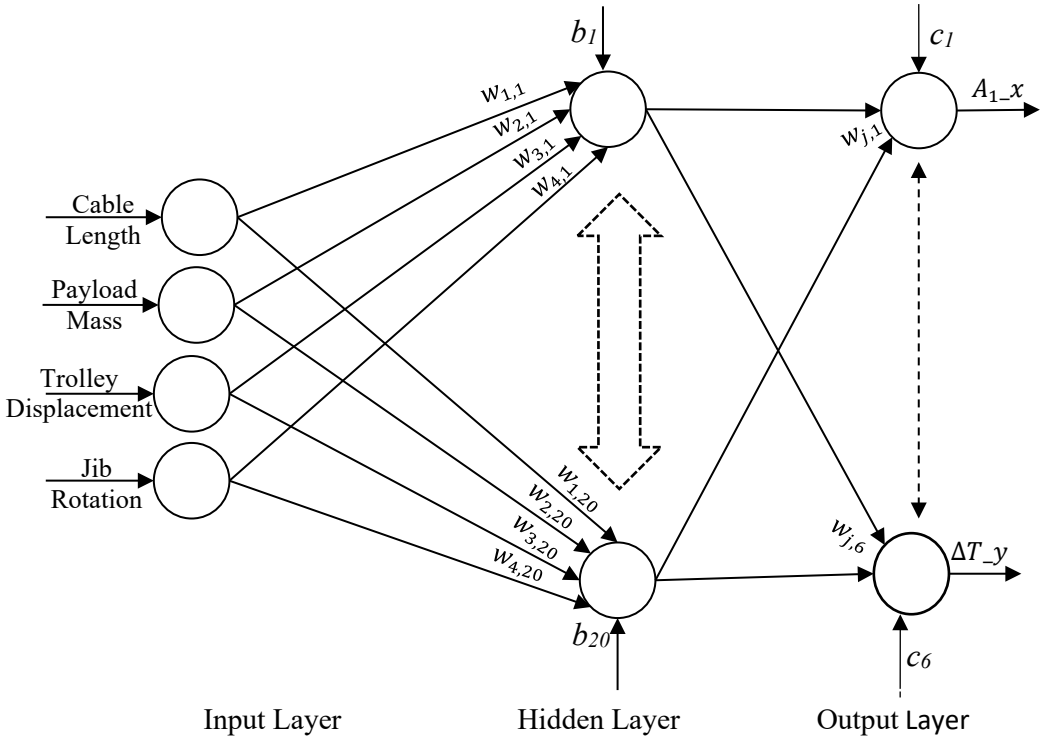

Figure 3: Bayesian Regularized Artificial Neural Network (BRANN)

Sigmoid activation function was used in the hidden layer due to the nonlinearity in the system under consideration and the wide range of measurements (cable length and trolley displacement in meter, payload mass in kilogram and jib rotation in radian). The ability of the sigmoid function to transfer any value between $\pm\propto$ to the corresponding value in the range of ± 1 also makes it an optimal choice. Figure 3 shows the NN structure where the indices i, j and k represent the input, hidden and output layers respectively. The output of any hidden neuron x_j can be calculated from the knowledge of its input x_i as

$$x_j = \text{Sigmoid}\left[\sum_{i=1}^{u} w_{i,j}x_i + b_j\right] \tag{10}$$

where $u = 4$ is the number of inputs. $w_{i,j}$ denotes the numerical weight of the link between the hidden and input neurons and b_j represents the bias value at the j-th hidden layer.

The output neurons used a linear activation function to calculate the target parameters and achieve better curve fitting. The function is also a better selection than the sigmoid function at output neurons as it gives the flexibility to take on any value. In this study, the ZVD delay

values can be higher than one second. The target values generated by the output neurons can be calculated as

$$y_k = \sum_{j=1}^{n} w_{j,k} x_j + c_k \tag{11}$$

where $n = 20$ is the number of hidden nodes. The weight value, $w_{j,k}$ is multiplied with the output of j-th neuron and then considered as the input of k-th node of the output layer. The predicted parameters are further tuned by adding the respective biased value, c_k in each output neuron thus generating an output closer to the target value. The six target values generated by the Bayesian Regularised Artificial Neural Network (BRANN) are $y_1 = A_1\_x$, $y_2 = A_3\_x$, $y_3 = A_1\_y$, $y_4 = A_2\_y$, $y_5 = \Delta T\_x$ and $y_6 = \Delta T\_y$. The weight values used by the trained NN between the input and hidden neurons, $w_{i,j}$ are depicted in Equation (12) and the link weights between hidden and output neurons, $w_{j,k}$ are given in Equation (13). As there are four input, 20 hidden and six output neurons, the size of the matrices for $w_{i,j}$ and $w_{j,k}$ are 4×20 and 20×6 respectively. Besides, the bias values are shown in Table 2.

$$\begin{bmatrix} w_{1,j} \\ w_{2,j} \\ w_{3,j} \\ w_{4,j} \end{bmatrix} = \begin{bmatrix} 0.007 & -3.458 & 0.0045 & \dots & 0.268 \\ 0.003 & 5.644 & -0.001 & \dots & -6.28 \\ 0.0045 & -4.609 & 0.002 & \dots & 1.707 \\ 0.0019 & -4.754 & -0.686 & \dots & 2.201 \end{bmatrix} \tag{12}$$

$$\begin{bmatrix} w_{j,1} & w_{j,2} & w_{j,3} & \dots & w_{j,6} \end{bmatrix} = \begin{bmatrix} 0.178 & -0.215 & 2.478 & \dots & -6.172 \\ 0.488 & -0.523 & 9.339 & \dots & 12.647 \\ 0.387 & 0.635 & -2.345 & \dots & 20.06 \\ \vdots & \vdots & \vdots & \vdots & \vdots \\ -0.416 & 0.407 & 1.252 & \dots & -1.415 \end{bmatrix} \tag{13}$$

Table 2: NN biased values for hidden and output layer neurons

b_j	-0.738	-13.917	-1.722	13.329	-4.166	-2.660	0.889	-14.043	. . .	0.858
c_k	2.584	-2.993	0.306	2.129	-2.101	-2.605				

4.2 EI Shaper Based on Average Operating Frequency (AOF)

Robustness of a ZV shaper can be enhanced by taking the derivatives of the residual vibration equation equal to zero which leads to the ZVD shaper. However, this additional robustness results in a slower system response. Each additional constraint requires an extra impulse to be convolved with the input, thus increases the shaper duration by 0.5 of the system's vibration period. To overcome this issue, EI shaper that has a higher robustness was proposed. The shaper

forces the residual vibration to zero at two different frequencies instead of a single modelling frequency [29]. The two frequencies are selected in a way that one is higher, and the other is lower than the modelling frequency. This technique helps EI to provide extra robustness against the parameter uncertainties while keeping the same shaper duration as of ZVD. Contrary to the ZVD in which the formulations were derived with the target to totally eliminate the residual swing, EI limits the residual to a tolerable value. It was reported that the ability of EI shaper to limit the residual vibration within 5% of residual swing is 140% better than the ZVD shaper [28].

The magnitudes and delays of the EI shaper can be determined as

$$\begin{bmatrix} A_i \\ t_i \end{bmatrix} = \begin{bmatrix} \frac{1+V_{tol}}{4} & \frac{1-V_{tol}}{2} & \frac{1+V_{tol}}{4} \\ 0 & \frac{\pi}{\omega_n\sqrt{1-\zeta^2}} & \frac{2\pi}{\omega_n\sqrt{1-\zeta^2}} \end{bmatrix} \tag{14}$$

where V_{tol} is the tolerable value and is normally taken as 0.05 or 5%.

As reported, EI exhibits higher robust performance towards parameter uncertainties as compared to ZV and ZVD shapers [29, 30]. Therefore, the EI shaper has been chosen to be the comparative method in this work. In addition, both ZVD and EI shapers require three-impulse sequence and with similar shaper duration. For a valid comparison, the robustness performance of the EI shaper was further improved by designing the shaper based on AOF. An average frequency of starting and final cable lengths along trolley and jib movements was considered and the shaper is referred as AOF-EI shaper. For each observation, two EI shapers were designed with 5% tolerable residual swing of payload for shaping the trolley and jib inputs. As the payload swing is affected by many factors, a dedicated AOF-EI shaper is required and it need to be re-designed for each scenario.

5. IMPLEMENTATION AND EXPERIMENTAL RESULTS

Real-time implementation on a laboratory tower crane and experimental results of the proposed NN-ZVD and robust AOF-EI shapers are presented in this section. The performance of both shapers to suppress the payload swing is examined in terms of overall and residual payload swings. The laboratory tower crane as shown in Figure 4 with dimensions of 1.2 m × 1.2 m × 1.5 m for its length, width and height respectively was used for experiments. The crane is connected to a computer through RT-DAC input output board. Payload swings

along x and y-axes, cable length, trolley displacement and jib rotation angle in the cylindrical plane are measured using optical encoders fitted in the tower crane. For the payload swing angle, the encoders are capable of measuring with an accuracy of 0.086 degrees. The motions of trolley, jib and payload hoisting are controlled using three DC motors while their speeds can be adjusted through the control signal communicated from the computer to the DC motor. The RT-DAC board is fitted with an FPGA-based Xilinx chip which is configured to generate appropriate sequence of pulse width modulation (PWM) signal to control speed of the DC motors. The data is send/receive via the RT-DAC board by using the Simulink interface C-source code and respective mex-files. Thus, user can define magnitude of the input signals and the respective PWM signals are generated by the configuration chips in the control board.

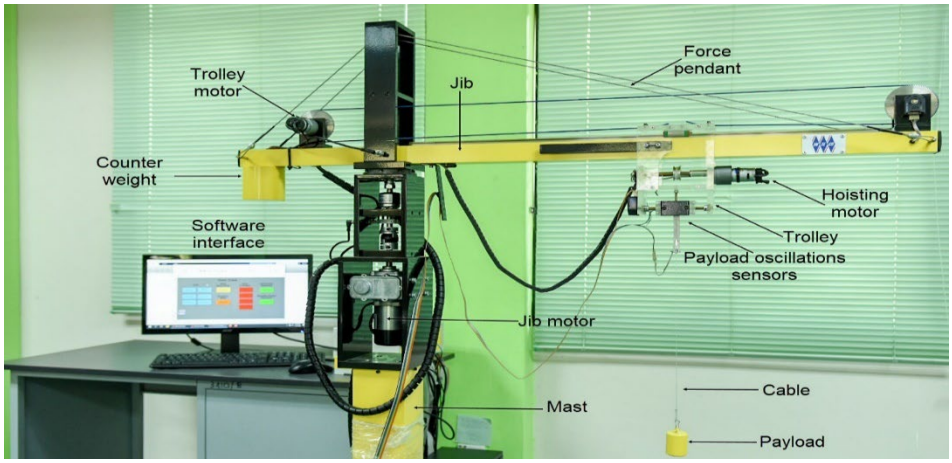

Figure 4: Laboratory tower crane

5.1 Performance Investigation

The capability of the proposed shaper to move the payload with minimum swing is examined under various scenarios and with simultaneous motions of the crane's parts. Experiments were performed on the laboratory crane with a maximum hoisting length of 0.8 m, trolley displacement of 0.5 m and jib rotation of 50 degrees. The payload mass of 200 g was used as a nominal weight while the shaper robustness was tested under $\pm$50% variations (100 g and 300 g) in payload mass. These scenarios provide changes up to 100% in the natural frequencies, which are crucial in input shaping design. It is worth mentioning that NN-ZVD performance was examined under conditions which were different from the one it was trained. Different combinations of payload masses, hoisting length, hoisting direction, trolley displacement and

jib rotation were considered to evaluate the shaper performance under all possible conditions. The performance of the shaper was quantitively measured by calculating the Mean Square Error (MSE) values for payload's overall and residual swings for the duration of 10 s and the last 1 s (from 9 s to 10 s) respectively. A lower value of MSE is preferable as it represents a smaller payload swing angle.

Three input forces applied by the DC motors were used to excite the trolley and jib (translational and slew) motions, and payload hoisting of the crane. As the payload swing response is affected by the motion speed, two input forces that produce different speeds are applied to investigate the performance of the shapers. These are referred to Case 1 and Case 2 in this work.

Case 1: The Trapezoidal Velocity Input

The trapezoidal input is a common velocity trajectory and most of industrial controllers work with this input [31, 32]. It is also known as the bang-cast-bang acceleration approach. This command arises when a human operator pushes a button or moves a joystick that causes a gradual increase in the velocity of crane trolley and jib until a maximum velocity is achieved. The crane continues to move with the maximum velocity until a stop command decelerates it back to zero, as shown in Figure 5(a). The trapezoidal velocity generates a more realistic industrial scenario which is important to be investigated.

Case 2: The Maximum Velocity Input

In this case, the trolley and jib are accelerated and decelerated with a maximum force as shown in Figure 5(b). The sudden change in motion of the crane from rest to motion and motion to rest induced intense oscillations in the payload. Moving the crane with a maximum speed is highly desirable as it minimises the payload transportation time but at the cost of a significant payload swing. Designing a time-efficient controller that can move the payload with minimum sway under a fast motion of crane can save valuable time normally wasted due to residual payload sway.

In addition to changes in the speed of motion, the robustness of the proposed controller was also examined with other parameters that affect the payload sways. Figure 6 shows the payload swing pendulation of the laboratory crane in x and y-axes. It can be shown that the magnitude and pattern of the pendulations are significantly affected with variations in payload masses, cable lengths, trolley displacement and jib rotation.

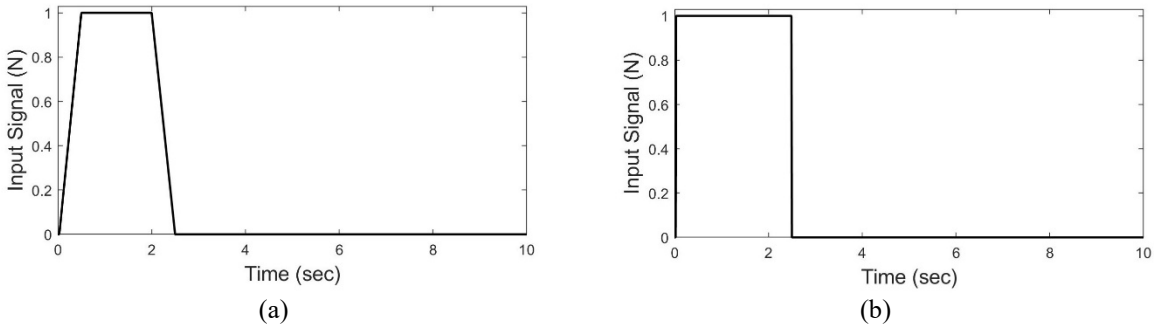

Figure 5: Tower crane inputs.

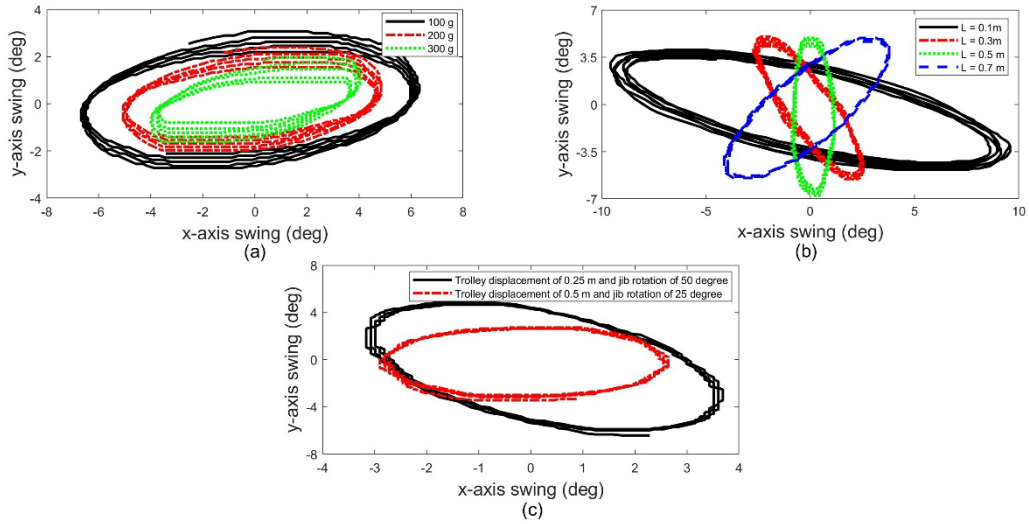

Figure 6: Payload swing with different (a) mass, (b) cable length, (c) trolley and jib displacements

In this work, simulations using the nonlinear model were carried out to collect data for input shaper design. Figure 7 shows the simulation and experimental results of the payload swing when the crane was excited with an input depicted in Figure 5(a). An acceptable agreement between both responses was obtained and thus the nonlinear model can be effectively used for controller design. A slight difference in the x and y-axes may be due to several factors such as air drag and friction which were not properly included in the dynamic model.

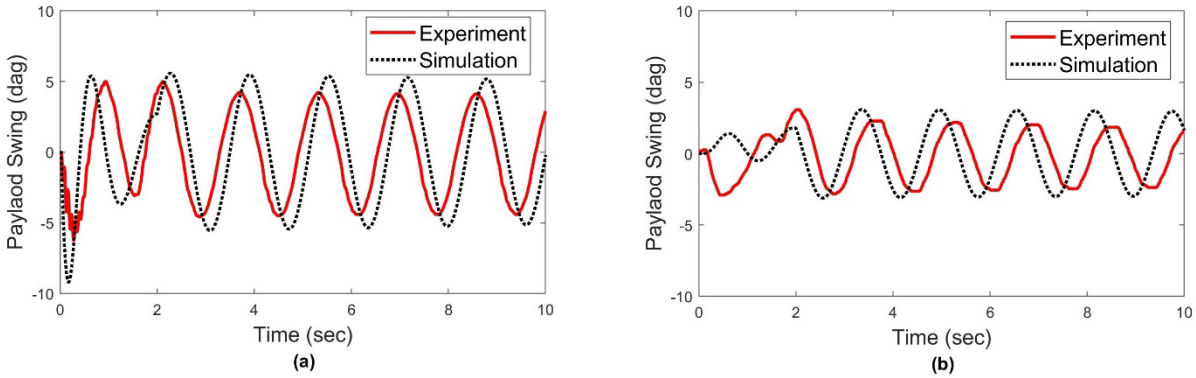

Figure 7: Simulation and experimental results of payload swing responses along (a) x-axis and (b) y-axis.

5.2 Experimental Results

This section presents experimental results based on the implementations of the proposed NN-ZVD and AOF-EI shapers on the laboratory tower crane.

5.2.1 Case 1: Trapezoidal Velocity Inputs

In this case, both the trolley and the jib were excited with the trapezoidal inputs shown in Figure 5(a) while the cable was hoisted at the maximum speed. Figure 8 shows 200 g payload pendulation when inputs of the tower crane were shaped with AOF-EI and the proposed NN-ZVD shapers. A condition with payload lowering from 0.1 m to 0.8 m, a trolley displacement of 0.4 m and a jib rotation of 40 degrees was considered and was referred as Case 1a. The result shows that NN-ZVD can significantly reduce the payload swing along both axes resulting in less than 0.5 degrees of residual swing.

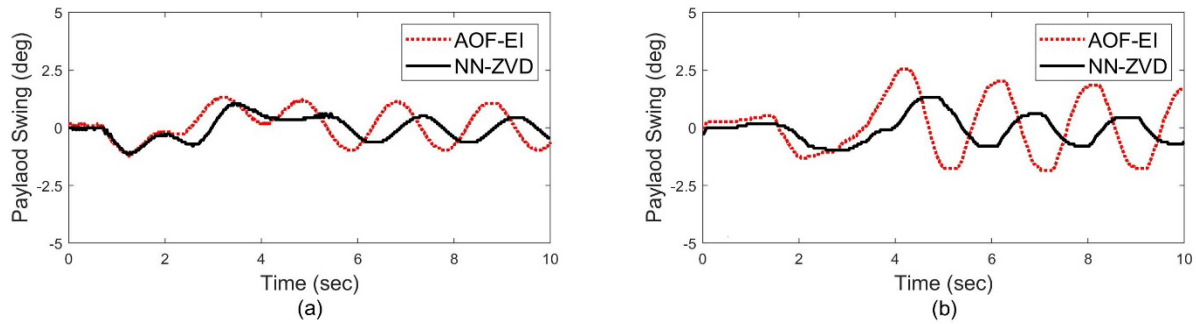

Figure 8: Swing response for Case 1a along (a) x-axis and (b) y-axis

To further investigate the robustness of the NN-ZVD shaper, the following operating conditions were considered:

- Case 1b: Payload 100 g, trolley displacement 0.5 m, jib rotation 25 degrees.
- Case 1c: Payload 300 g, trolley displacement 0.25 m, jib rotation 50 degrees.
- Case 1d: Payload 100 g, trolley displacement 0.5 m, jib rotation 25 degrees.
- Case 1e: Payload 200 g, trolley displacement 0.4 m, jib rotation 40 degrees.

Cases 1b and 1c involve payload lowering from 0.1 m to 0.8 m and their payload swing responses are shown in Figure 9. Besides, Cases 1d and 1e examine the payload lifting from 0.8 m to 0.1 m, with similar trolley displacements and jib rotations as in the previous conditions (payload lowering). The payload swing responses are shown in Figure 10. It is important to mention for each case, a separate AOF-EI shaper needs to be designed as the pendulation dynamics change. However, a single NN-ZVD shaper was used for all conditions without the requirement for re-design. The results show that NN-ZVD can limit the residual vibration within ±1 degree irrespective of the variations in the parameters. For the cases with payload lifting, the NN-ZVD also proved its robustness by limiting the payload swing within the range of ±0.5 degrees whereas the AOF-EI shaper performance degraded. The quantitative measures of all scenarios in terms of MSE values of overall and residual swings are shown in Table 3. Moreover, the percentage improvements of NN-ZVD over AOF-EI are shown in Figure 11. In all cases, the NN-ZVD achieved at least 50% improvements over AOF-EI.

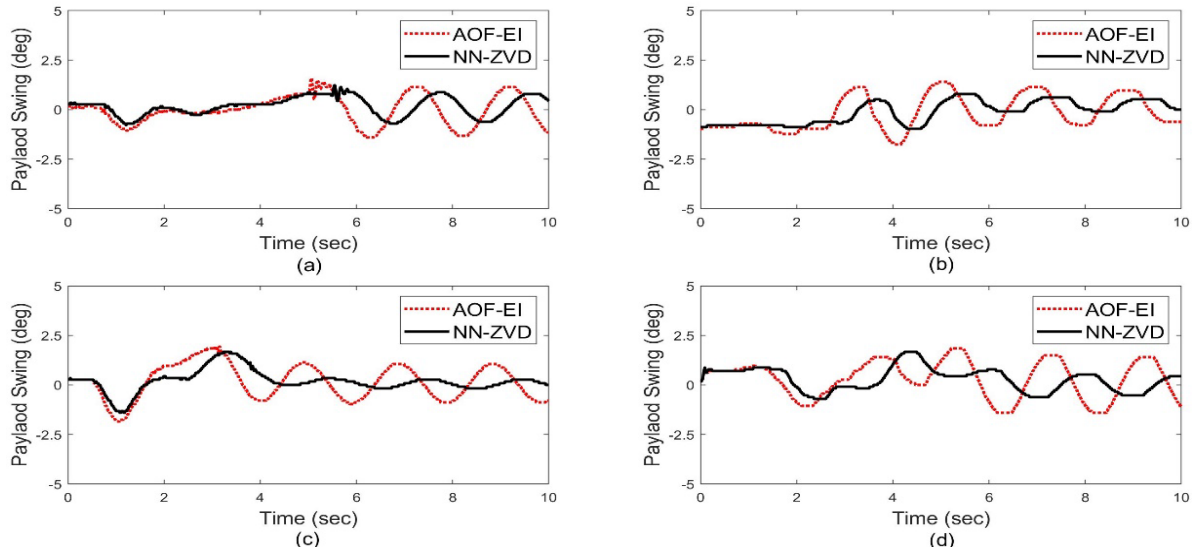

Figure 9: Swing response for Case 1b (a,b) and Case 1c (c,d) along (a,c) x-axis and (b,d) y-axis.

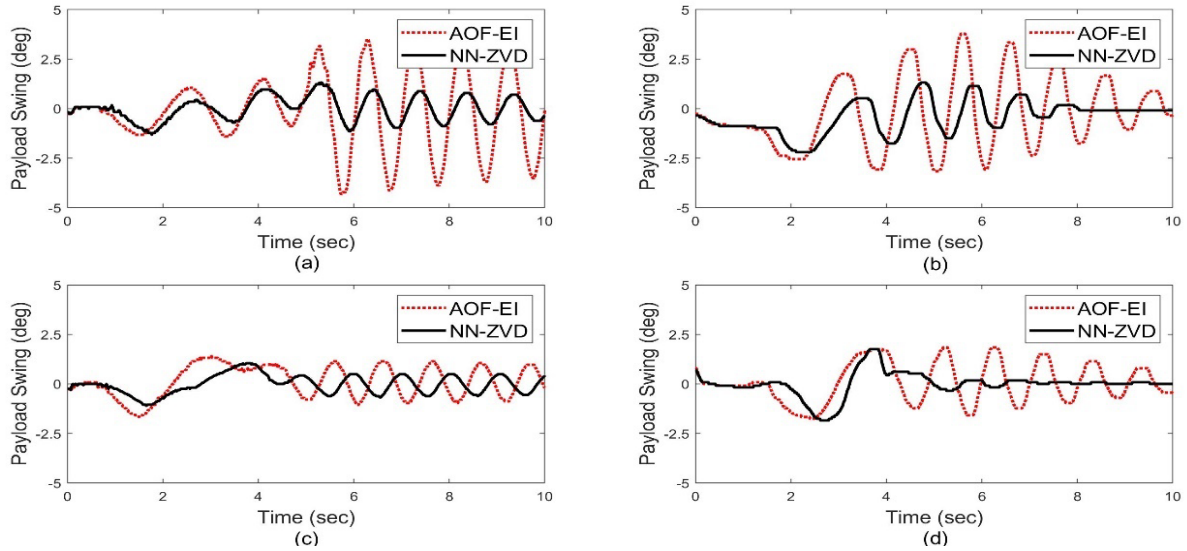

Figure 10: Swing response for Case 1d (a,b) and Case 1e (c,d) along (a,c) x-axis and (b,d) y-axis.

Table 3: MSE values of payload swing with NN-ZVD and AOF-EI shapers using the trapezoidal input

Case	Axis	Overall swing (MSE)		Residual swing (MSE)	
		NN-ZVD	AOF-EI	NN-ZVD	AOF-EI
Case 1a	x	0.35	0.78	0.18	0.36
	y	0.26	0.51	0.36	0.75
Case 1b	x	0.26	0.53	0.12	0.48
	y	0.37	1.57	0.28	1.72
Case 1c	x	0.34	0.80	0.14	0.44
	y	0.42	0.96	0.15	1.12
Case 1d	x	0.39	3.50	0.24	5.11
	y	0.87	3.26	0.01	0.49
Case 1e	x	0.33	0.66	0.20	0.46
	y	0.39	1.01	0.002	0.26

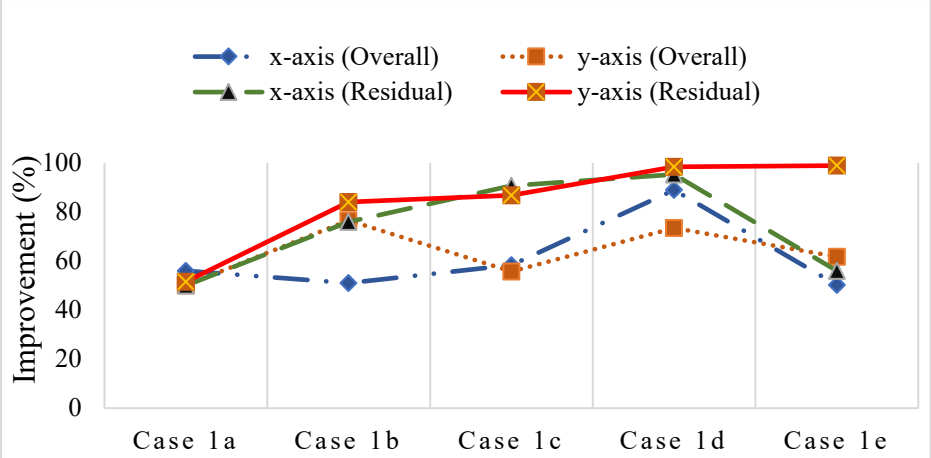

Figure 11: Percentage improvements of NN-ZVD over AOF-EI

5.2.2 Case 2: Maximum Velocity Inputs

A fast crane movement is highly desirable to speed up the operation process, but it is at the cost of higher payload swing. To achieve both the minimum transportation time and low payload swing controller, the shaper parameters need to be updated accurately in real-time. In this section, experimental results of the payload swing responses with the input force as shown in Figure 5(b) are presented. The following conditions were observed:

- Case 2a: Payload 200 g, trolley displacement 0.21 m, jib rotation 20 degrees, payload lowering 0.1 m to 0.4 m.
- Case 2b: Payload 100 g, trolley displacement 0.45 m, jib rotation 45 degrees, payload lowering 0.1 m to 0.76 m.
- Case 2c: Payload 300 g, trolley displacement 0.3 m, jib rotation 30 degrees, payload lowering 0.1 m to 0.54 m.

The results for Case 2a are shown in Figure 12 which demonstrate that NN-ZVD is more capable of suppressing the payload swings despite a higher motion speed. In particular, for the y-axis, the NN-ZVD can almost completely eliminate the payload swing. Figures 13 shows the results for Cases 2b and 2c which displayed a similar pattern. In all cases, the residual payload swings were kept within 1 degree with the NN-ZVD shaper.

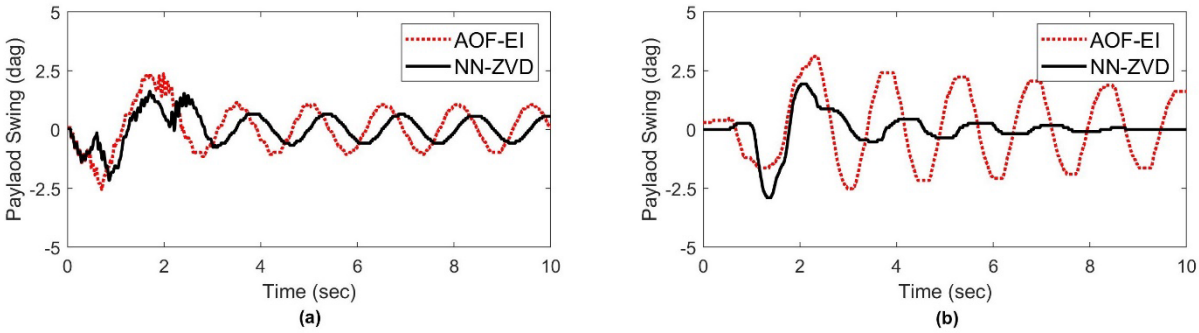

Figure 12: Swing response for Case 2a along (a) x-axis and (b) y-axis.

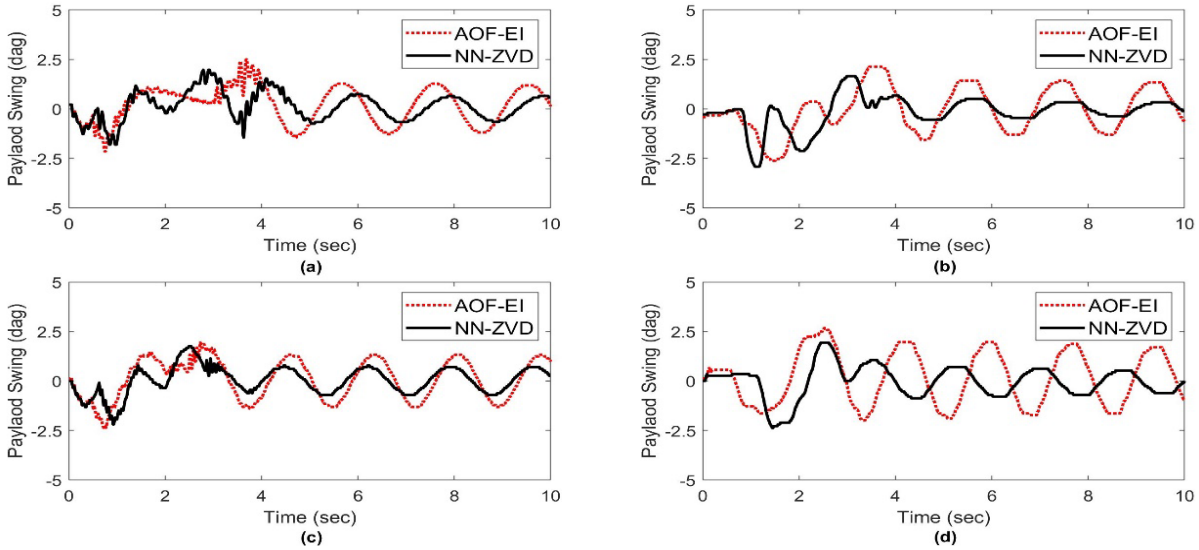

Figure 13: Swing response for Case 2b (a,b) and Case 2c (c,d) along (a,c) x-axis and (b,d) y-axis.

In spite of moving the crane with a maximum speed, comparisons of MSE values in Table 4 show that a single NN-ZVD shaper achieves a superior performance as compared to dedicated AOF-EI shapers. Improvements of NN-ZVD over AOF-EI are presented in Figure 14, which is more than 50% in the overall swing and with a minimum improvement of 71% in the residual swing.

Table 4: MSE values of the payload swing response with NN-ZVD and AOF-EI shapers using the maximum velocity

Case	Axis	Overall swing (MSE)		Residual swing (MSE)	
		NN-ZVD	AOF-EI	NN-ZVD	AOF-EI
Case 2a	x	0.43	0.91	0.22	0.77
	y	0.65	1.36	0.12	1.25
Case 2b	x	0.45	0.92	0.19	0.49
	y	0.53	2.47	0.0002	1.83

Case 2c	x	0.49	1.04	0.25	0.91
	y	0.67	1.88	0.20	1.50

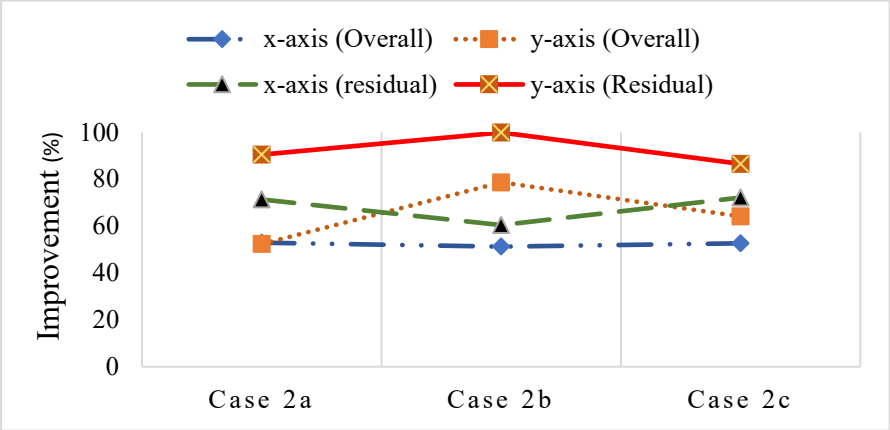

Figure 14: Percentage improvements of NN-ZVD over AOF-EI

5.3 Obstacle Avoidance

Another challenging practical scenario is to avoid an obstacle during a crane operation. When there is an obstacle in between the start and end positions, the operator has two choices: to avoid a collision by navigating the payload around the obstacle or perform a combination of hoisting operations. Many researchers have devised mechanisms to avoid the collision by adopting a nominal path, but it requires more complex calculations with a longer path. In some cases, the obstacle was avoided by considering only hoisting up operation and with a slower crane motion [33]. A good control mechanism for a tower crane under this scenario is still lacking.

In this work, a more complex scenario was considered by moving the crane with a maximum force while the collision is avoided by performing an appropriate combination of lifting and lowering maneuverings. Eliminating the payload swing is difficult when a combination of payload hoisting up-down is performed in a single manoeuvre. Figure 15 shows front and top views of a scenario with an obstacle of 0.45 m height. Two payload's initial conditions of 0.7 m and 0.2 m from the trolley were considered and the target position in both conditions was 0.8 m. Figures 16(a) and 16(b) show the cable length variations in carrying the tasks. As this scenario also considered simultaneous motions, the payload path was pre-planned by considering the trolley translational and jib rotation speeds, to ensure that the payload is lifted to a safety height before it is lowered to the desired position.

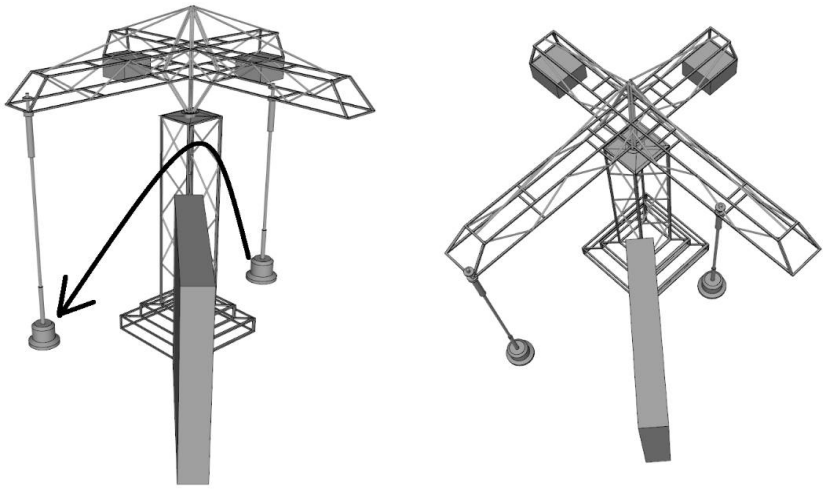

(a) (b)

Figure 15: An obstacle in between of initial and final locations of the payload with (a) front view and (b) top view

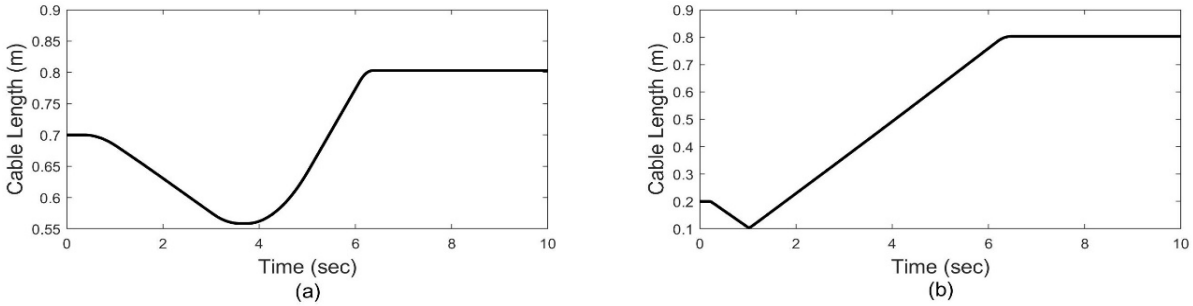

Figure 16: Cable length hoisting for obstacle avoidance with different payload's initial conditions (a) 0.7 m (b) 0.2 m

Figure 17 shows payload swing responses of the laboratory crane with a payload of 200 g. In both conditions, the trolley and jib were simultaneously moved to 0.3 m and 30 degrees respectively. The results confirmed that the proposed NN-ZVD shaper has a higher robustness over the AOF-EI shaper by limiting the residual payload swing to ±1 degree. Table 5 presents the MSE values of the payload swing achieved using both shapers. It is noted that NN-ZVD provided a better response and with a minimum improvement of 50%.

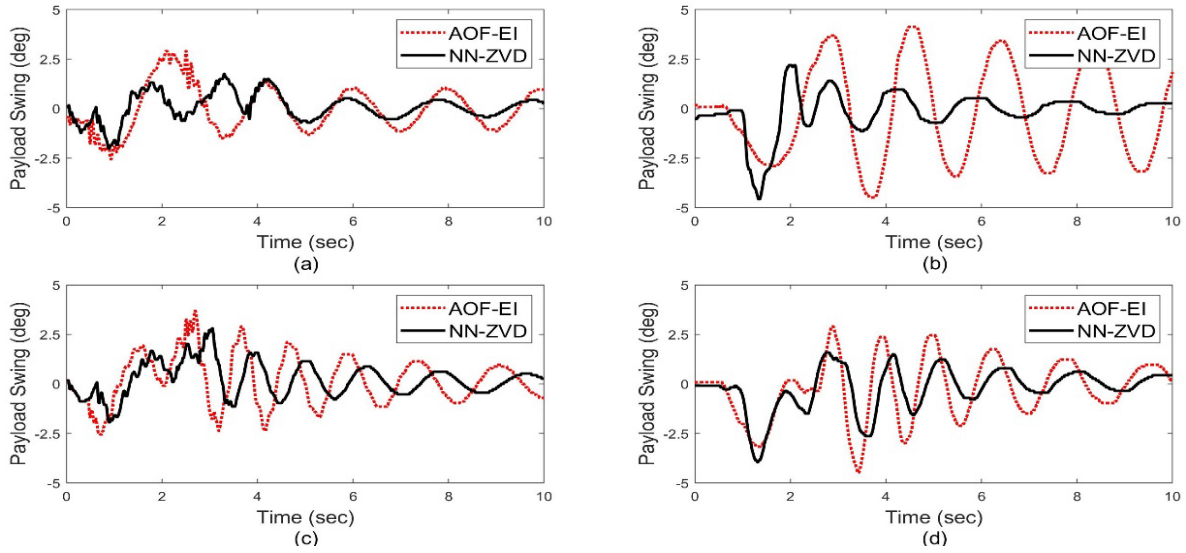

Figure 17: Payload swing with obstacle avoidance (a,b) initial condition of 0.7 m, (c,d) initial condition of 0.2 m, along (a,c) x-axis and (b,d) y-axis

Table 5: MSE values of payload swing response with NN-ZVD and AOF-EI shapers under obstacle avoidance

Initial condition (m)	Axis	Overall swing			Residual swing		
		NN-ZVD (MSE)	AOF-EI (MSE)	Imp (%)	NN-ZVD (MSE)	AOF-EI (MSE)	Imp (%)
0.2	x	0.4719	1.3053	63.85	0.0925	0.5598	83.48
	y	1.1337	5.9946	81.09	0.0478	5.3935	99.11
0.7	x	0.768	1.6144	52.43	0.1363	0.3946	65.45
	y	1.2212	2.3859	48.82	0.1198	0.5285	77.32

Imp - Improvement

A clearer view on the payload's circular pendulations during the crane motions to avoid the obstacle can be shown by plotting the swing in x and y-axes. Figure 18 shows the circular motions using the unshaped and shaped inputs under both initial conditions. It is also a top view of the motions. It is noted that the shape of the pendulations were different in both conditions and the unshaped input resulted in a very large sway area. Nevertheless, similar to the previous results, the NN-ZVD shaper achieved the best performance with the smallest area of sway. Experimental results demonstrate that the proposed adaptive shaper is able to handle changing cable lengths through payload lifting and lowering within a single manoeuvre, and together with simultaneous and fast trolley and jib rotation motions.

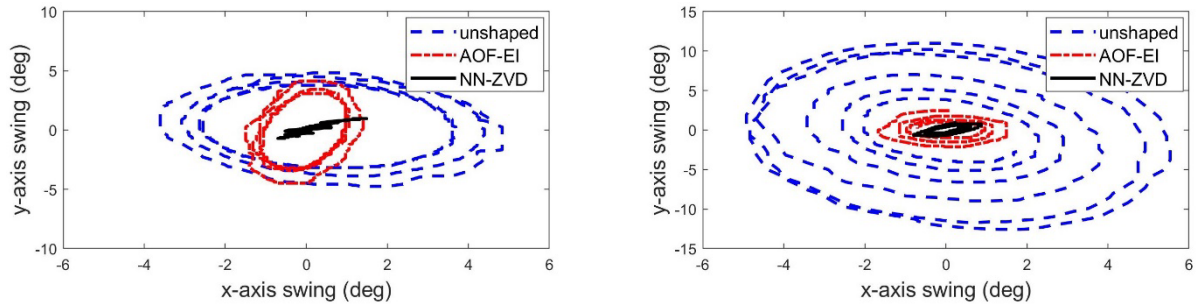

Figure 18: Payload pendulations of a 200 g payload with obstacle avoidance, (a) initial condition of 0.7 m, (b) initial condition of 0.2 m.

6. CONCLUSIONS

An adaptive input shaper has been designed and implemented in real time for payload swing control of a 5-DOF tower crane under parameter uncertainties, payload hoisting and with simultaneous motions of crane's parts. The capability of NN to generate a nonlinear input-output mapping has been utilised to develop an adaptive mechanism in which optimal shaper's parameters can be continuously updated according to the changes in the crane dynamics. Experiments under challenging practical scenarios up to 100% changes in the payload sway frequencies have demonstrated the superiority of the NN-ZVD shaper over the robust AOF-EI shaper. In all cases, at least 50% improvements have been achieved using the NN-ZVD, and the residual sway has been kept less than one degree. Moreover, a satisfactory performance has also been achieved under an obstacle avoidance scenario. Future research will consider implementation of the proposed technique on a tower crane with double-pendulum dynamics. This type of crane is closer to the real practical crane, but its swing control is challenging as hook and payload sways need to be considered, and they oscillate with difference frequencies. It is also envisaged that the proposed shaper design can be implemented for payload swing control of other crane systems with translational and rotational motions.

REFERENCES

[1] T.Y.T. Kuo, S.C.J. Kang, Control of fast crane operation, Automation in Construction 42 (2014) pp. 25-35 , doi:10.1016/j.autcon.2014.02.003.

[2] A.T. Le, S.-G. Lee, 3D cooperative control of tower cranes using robust adaptive techniques, Journal of the Franklin Institute 354(18) (2017) pp. 8333-8357, doi: 10.1016/j.jfranklin.2017.10.026.

[3] T.-S. Wu, M.A. Karkoub, H. Wang, H.-S. Chen, T.-H. Chen, Robust tracking control of MIMO underactuated nonlinear systems with dead-zone band and delayed uncertainty using an adaptive fuzzy control, IEEE Transactions on Fuzzy Systems 25 (2017) pp. 905-918, doi: 10.1109/TFUZZ.2016.2586970.

[4] Y. Qian, Y. Fang, Switching logic-based nonlinear feedback control of offshore ship-mounted tower cranes: A disturbance observer-based approach, IEEE Transactions on Automation Science and Engineering 16(3) (2019) pp. 1125-1136, doi: 10.1109/TASE.2018.2872621.

[5] N. Sun, Y. Wu, H. Chen, Y. Fang, Antiswing cargo transportation of underactuated tower crane systems by a nonlinear controller embedded with an integral term, IEEE Transactions on Automation Science and Engineering 16(3) (2019) pp. 1387-1398, doi: 10.1109/TASE.2018.2889434.

[6] Š. Ileš, J. Matuško, F. Kolonić, Sequential distributed predictive control of a 3D tower crane, Control Engineering Practice 79 (2018) pp. 22-35, doi: 10.1016/j.conengprac.2018.07.001.

[7] M. Bock, A. Kugi, Real-time nonlinear model predictive path-following control of a laboratory tower crane, IEEE Transactions on Control Systems Technology 22(4) (2014) pp. 1461-1473, doi: 10.1109/TCST.2013.2280464.

[8] M. Zhang, X. Jing, Z. Zhu, Disturbance employment-based sliding mode control for 4-DOF tower crane systems, Mechanical Systems and Signal Processing 161 (2021) 107946, doi: 10.1016/j.ymssp.2021.107946.

[9] M.H. Zhang, X.J. Jing, Model-free saturated PD-SMC method for 4-DOF tower crane systems, IEEE Transactions on Industrial Electronics 69(10) (2022) pp. 10270-10280. doi : 10.1109/TIE.2021.3139134.

[10] P. Van Trieu, H.M. Cuong, H.Q. Dong, N.H. Tuan, L.A. Tuan, Adaptive fractional-order fast terminal sliding mode with fault-tolerant control for underactuated mechanical systems: Application to tower cranes, Automation in Construction 123 (2021) 103533, doi: 10.1016/j.autcon.2020.103533.

[11] T.-S Wu, M. Karkoub, W.S. Yu, C.T. Chen, M.G. Her, K.W. Wu, Anti-sway tracking control of tower cranes with delayed uncertainty using a robust adaptive fuzzy control, Fuzzy Sets and Systems 290 (2016) pp. 118–137, doi: 10.1016/j.fss.2015.01.010.

[12] Z. Sun, H. Ouyang, Adaptive fuzzy tracking control for vibration suppression of tower crane with distributed payload mass, Automation in Construction 142 (2022) 104521, doi: 10.1016/j.autcon.2022.104521.

[13] S. Cho, S. Han, Reinforcement learning-based simulation and automation for tower crane 3D lift planning, Automation in Construction 144 (2022) 104620, doi: 10.1016/j.autcon.2022.104620.

[14] L. Ramli, I.M. Lazim, H.I. Jaafar, Z. Mohamed, Modelling and fuzzy logic control of an underactuated tower crane system, Applications of Modelling and Simulation 4 (2020) pp. 1-11.

[15] M. Zhang, Y. Zhang, B. Ji, C. Ma, X. Cheng, Adaptive sway reduction for tower crane systems with varying cable lengths, Automation in Construction 119 (2020) 103342, doi: 10.1016/j.autcon.2020.103342.

[16] H. Chen, Y. Fang, N. Sun, An adaptive tracking control method with swing suppression for 4-DOF tower crane systems, Mechanical Systems and Signal Processing 123 (2019) pp. 426-442, doi: 10.1016/j.ymssp.2018.11.018.

[17] T. Yang, N. Sun and Y. Fang, Neuroadaptive control for complicated underactuated systems with simultaneous output and velocity constraints exerted on both actuated and unactuated states, IEEE Transactions on Neural Networks and Learning Systems (2021) pp. 1-11, doi: 10.1109/TNNLS.2021.3115960.

[18] J.-H. Montonen, N. Nevaranta, M. Niemelä, T. Lindh, Comparison of extrainsensitive input shaping and swing-angle-estimation-based slew control approaches for a tower crane, Applied Sciences 12(12) (2022) 5945, doi: 10.3390/app12125945.

[19] S.M. Fasih, Z. Mohamed, A.R. Husain, L. Ramli, A.M. Abdullahi, W. Anjum, Payload swing control of a tower crane using a neural network–based input shaper, Measurement and Control 53(7-8) (2020) pp. 1171-1182, doi: 10.1177/0020294020920895.

[20] S.M. Fasih ur Rehman, Z. Mohamed, A.R. Husain, H.I. Jaafar, M.H. Shaheed, M.A. Abbasi, Input shaping with an adaptive scheme for swing control of an underactuated tower crane under payload hoisting and mass variations, Mechanical Systems and Signal Processing 175 (2022) 109106, doi: 10.1016/j.ymssp.2022.109106.

[21] A. Al-Fadhli, E. Khorshid, Payload oscillation control of tower crane using smooth command input, Journal of Vibration and Control 29(3-4) (2021) pp. 902-915, doi: 10.1177/1077546321105464.

[22] J. Ye, J. Huang, Control of beam-pendulum dynamics in a tower crane with a slender jib transporting a distributed-mass load, IEEE Transactions on Industrial Electronics 70(1) (2023) pp. 888-897, doi: 10.1109/TIE.2022.3148741.

[23] J.J. Wilbanks, M.J. Leamy, Robust two-scale command shaping for residual vibration mitigation in nonlinear systems, Journal of Sound and Vibration 462 (2019) 114927, doi: 10.1016/j.jsv.2019.114927.

[24] L. Ramli, Z. Mohamed, H.I. Jaafar, A neural network-based input shaping for swing suppression of an overhead crane under payload hoisting and mass variations, Mechanical Systems and Signal Processing 107 (2018) pp. 484-501, doi: 10.1016/j.ymssp.2018.01.029.

[25] M.J. Maghsoudi, Z. Mohamed, A.R. Husain, M.O. Tokhi, An optimal performance control scheme for a 3D crane, Mechanical Systems and Signal Processing 66-67 (2016) pp. 756-768, doi: 10.1016/j.ymssp.2015.05.020.

[26] H.I. Jaafar, Z. Mohamed, M.A. Ahmad, N.A. Wahab, L. Ramli, M.H. Shaheed, Control of an underactuated double-pendulum overhead crane using improved model reference command shaping: Design, simulation and experiment, Mechanical Systems and Signal Processing 151 (2021) 107358, doi: 10.1016/j.ymssp.2020.107358.

[27] W. Singhose, L. Porter, M. Kenison, E. Kriikku, Effects of hoisting on the input shaping control of gantry cranes, Control Engineering Practice 8(10) (2000) pp. 1159-1165, doi: 10.1016/S0967-0661(00)00054-X.

[28] W. Singhose, Command shaping for flexible systems: A review of the first 50 years, International Journal of Precision Engineering and Manufacturing 10(4) (2009) pp. 153-168, doi: 10.1007/s12541-009-0084-2.

[29] W. Singhose, S. Derezinski, N. Singer, Extra-insensitive input shapers for controlling flexible spacecraft, Journal of Guidance, Control and Dynamics 19(2) (1996) pp. 385-391, doi: 10.2514/3.21630.

[30] J. Vaughan, A. Yano, W. Singhose, Comparison of robust input shapers, Journal of Sound and Vibration 315(4) (2008) pp. 797-815, doi: 10.1016/j.jsv.2008.02.032.

[31] N. Uchiyama, H. Ouyang, S. Sano, Simple rotary crane dynamics modeling and open-loop control for residual load sway suppression by only horizontal boom motion, Mechatronics 23(8) (2013) pp. 1223-1236, doi: 10.1016/j.mechatronics.2013.09.001.

[32] R. Tang, J. Huang, Control of bridge cranes with distributed-mass payloads under windy conditions, Mechanical Systems and Signal Processing 72-73 (2016) pp. 409-419, doi: 10.1016/j.ymssp.2015.11.002.

[33] K.L. Sorensen, W. Singhose, S. Dickerson, A controller enabling precise positioning and sway reduction in bridge and gantry cranes, Control Engineering Practice 15(7) (2007) pp. 825-837, doi: 10.1016/j.conengprac.2006.03.005.